High-performance asymmetric supercapacitor based on vanadium dioxide and carbonized iron-polyaniline electrodes

Cite as: AIP Advances **9**, 055309 (2019); https://doi.org/10.1063/1.5091799
Submitted: 05 February 2019 . Accepted: 29 April 2019 . Published Online: 10 May 2019

N. M. Ndiaye, M. J. Madito, B. D. Ngom, T. M. Masikhwa, A. A. Mirghni, and N. Manyala

High-performance asymmetric supercapacitor based on vanadium dioxide and carbonized iron-polyaniline electrodes

Cite as: AIP Advances 9, 055309 (2019); doi: 10.1063/1.5091799
Submitted: 5 February 2019 • Accepted: 29 April 2019 •
Published Online: 10 May 2019

N. M. Ndiaye,[1] M. J. Madito,[1] B. D. Ngom,[2] T. M. Masikhwa,[1] A. A. Mirghni,[1] and N. Manyala[1,a)]

AFFILIATIONS

[1] Department of Physics, Institute of Applied Materials, SARChI Chair in Carbon Technology and Materials, University of Pretoria, Pretoria 0028, South Africa

[2] Laboratoire de Photonique Quantique d'Energie et de Nano Fabrication, Groupe de Physique du Solide et Science des Matériaux, Département de Physique FST-UCAD BP 5005 Dakar-Fan, Dakar, Sénégal

[a)] **Corresponding author email:** ncholu.manyala@up.ac.za, **Tel.:** + (27)12 420 3549 **Fax:** + (27)12 420 2516

ABSTRACT

Vanadium dioxide (VO_2) monoclinic nanosheets were synthesized by a solvothermal method and carbonized iron-polyaniline (C-FP) nanograins were prepared by pyrolysis of iron-polyaniline (PANI) mixture under nitrogen ambient. An asymmetric device (VO_2//C-FP) was evaluated with VO_2 and C-FP as positive and negative material electrodes in aqueous 6 M KOH electrolyte respectively. The asymmetric supercapacitor (VO_2//C-FP) exhibited a 47 mA h g^{-1} specific capacity and a specific energy of 30 W h kg^{-1} with an associated specific power of 713 W kg^{-1} at a gravimetric current of 1 A g^{-1} in a potential window of 1.6 V. It also displayed an 89% energy efficiency after 10000 galvanostatic charge-discharge cycles with a large improvement after ageing test at a gravimetric current of 10 A g^{-1}.

I. INTRODUCTION

Supercapacitors (SCs), also called electrochemical capacitors (ECs) have been on the forefront of research owing to their relatively high power density (15 kW kg^{-1}), low specific energy (<10 W h kg^{-1}) and a long lifetime.[1–6] To date, the scientific community is working towards increasing the specific energy of SCs by using ingenious device design.[7] SCs can be classified into three types of capacitors based on their charge storage mechanism: (i) The electrical double-layer capacitors (EDLCs), where charge build-up at the boundary between the electrode and the electrolyte is responsible for the energy storage and the common materials used are carbon-based materials.[2,8] (ii) The faradaic capacitor which as their names suggest, involve redox or faradaic reaction and is mainly displayed in transition metal oxides, metal hydroxides, metal sulfides and conducting polymers.[9–13] (iii) The hybrid capacitors which are the combination of both EDLC and faradaic materials. A subclass of hybrid capacitors is the asymmetric supercapacitor (ASC) which are composed of a positive and a negative electrodes with dissimilar charge storage mechanisms. Generally, the positive electrodes are the faradaic materials[14–21] while the negative electrodes are mostly made of carbon-based materials.[22–26] The Hybrid capacitors have been proposed and considered as a promising solution to improve the low specific capacitance from carbon-based materials and the low conductivity and poor cycle stability of the transition metal oxides/hydroxides.[27]

Carbon-based materials such as activated carbon,[28] carbon nanotube[29] and graphene[30] have been demonstrated to be a good electrode materials in supercapacitor due to their excellent conductivity combined with their good stability.[31]

The transition metal oxide used as supercapacitor electrode materials exhibit a high specific capacity as compared to carbon-based materials owing to its multiple oxidations states.

Amongst the low-cost metal oxides, vanadium oxides (e.g. VO_2, V_2O_5, V_2O_3, and V_4O_7) have received recent attention[32–40] which is linked to their abundant sources, and ability to exist in variable oxidation states.[41]

Vanadium dioxide (VO_2) has an exciting phase with a rich polymorphic stable and metastable forms included VO_2 (A), VO_2 (M), VO_2 (R), VO_2 (B), VO_2 (T) and VO_2 (bcc).[42,43] VO_2 (A),

VO_2 (M) and VO_2 (B) are the most attractive due to their tuneable and the relatively easy synthesis process.[42,44] The VO_2 materials change from monoclinic (at a temperature about 68°C) to tetragonal structure reversibly (at a temperatures higher than the 68 °C) and can undergo semiconductor-to-metal transition.[45–50] VO_2 (B) electrodes with a metastable monoclinic structure is a potential electrode material in supercapacitor.[51]

As compared to vanadium pentoxide (V_2O_5), there are few report on vanadium dioxide for asymmetric supercapacitor. For instance, Wang et al. synthesized a graphene/VO_2 composite material for a positive and a negative electrodes. They assembled a symmetric supercapacitor (graphene/VO_2//graphene/VO_2) using 0.5 M Na_2SO_4 as an aqueous electrolyte. The graphene/VO_2//graphene/VO_2 symmetric device showed a specific energy of 21.3 W h kg^{-1} at 1 A g^{-1}. The graphene/VO_2 composite showed a cycling stability with 92% after 5000th cycles at 10 A g^{-1}.[52] Similarly Ma et *al.*[48] prepared a vanadium dioxide electrode using for a symmetric supercapacitor in 1 M Na_2SO_4. The VO_2//VO_2 symmetric device exhibited a specific energy of 21.3 W h kg^{-1} corresponding to a specific power of 207.2 W kg^{-1} at a gravimetric current of 0.25 A g^{-1}. They reported a cycling efficiency of 78.7% after 5.000 cycles at a specific current of 0.5 A g^{-1}.[48]

In our previous study, we synthesized the vanadium dioxide monoclinic (VO_2 (B)) through a solvothermal method. In a three electrode configuration the VO_2 (B) displayed a specific capacity of 49.28 mAh g^{-1} at current density of 0.5 A g^{-1} in aqueous electrolyte (6 M KOH).[53]

The present work reports the fabrication of a novel asymmetric supercapacitor (ASC) based on VO_2 (B) monoclinic as a positive electrode and carbonized iron-polyaniline (C-FP) as a negative electrode. The VO_2//C-FP ASC tested in aqueous electrolyte (6 M KOH) was able to reach a potential window of 1.6 V. The asymmetric device exhibited a specific energy and power of 30 W h kg^{-1} and 713 W kg^{-1} respectively at 1 A g^{-1}. In addition, the ASC showed an 89% energy efficiency after 10000 galvanostatic charge-discharge cycles with a large improvement after ageing test at a gravimetric current of 10 A g^{-1}.

II. EXPERIMENTAL

A. Chemicals

Vanadium (V) oxide (V_2O_5, purity ≥98%), oxalic acid dehydrate ($C_2H_2O_4{\cdot}2H_2O$ purity 99%), iron (III) nitrate ($Fe(NO_3)_3{\cdot}9H_2O$ purity 99-100%), ammonium peroxydisulfate ($(NH_4)_2S_2O_8$) purity 98%), aniline hydrochloride ($C_6H_5NH_2{\cdot}HCl$ purity ≥99%) and propan-2-ol ($CH_3CHOHCH_3$ purity 99.5%) were purchased from Sigma-Aldrich. Potassium hydroxide (KOH) and ethanol (C_2H_6O purity 99%) were purchased from Merck (South Africa). Polycrystalline nickel foam (thickness of 1.6 mm) was obtained from Alantum (Munich, Germany).

B. Synthesis technique

1. Preparation of vanadium dioxide (VO_2)

The synthesis of the VO_2 material was carried out using solvothermal method. Initially, 1.2 g of V_2O_5 powder and 2.49 g of $H_2C_2O_4{\cdot}2H_2O$ was added to 40 mL of deionized water and stirred for 3 h, thereafter, a 6 mL of the homogeneous solution was added to 60 mL of isopropanol under continuous stirring for 20 min.

The solution was transferred into a Teflon-lined stainless steel autoclave and kept at 200 °C for 6 h. The recovered powder was washed several times with deionized water followed by ethanol and dried at 60 °C in an electric oven.[53]

2. Synthesis of polyaniline (PANI)

0.2 M aniline hydrochloride ($C_6H_5NH_2{\cdot}HCl$) (2.59 g dissolved in 50 mL deionized water) was added to 0.25 M ammonium peroxydisulfate ($(NH_4)_2S_2O_8$) (5.71 g in 50 mL deionized water) and mixed overnight.

3. Preparation of carbonized iron-PANI (C-FP)

Briefly, 0.2 g of $Fe(NO_3)_3{\cdot}9H_2O$ and 0.0125 g of PANI were dissolved in 50 ml of ethanol and sonicated in the ultra-sonication bath.

After ethanol was almost completely evaporated, the mixture was coated on a nickel (Ni) foam acting as a current collector and pyrolyzed for 2 h under the N_2 atmosphere at 850 °C. The full detailed description of the C-FP can be found in our previous paper.[54]

C. Structural characterization

The structural properties of the samples were analysed by X-ray diffraction (XRD) powder using an XPERT-PRO diffractometer (PANalytical BV, The Netherlands) with theta/2theta configuration. The morphology of the materials synthesized was characterized by a high-resolution Zeiss Ultra plus 55 field emission scanning electron microscope (FE-SEM), operated at a voltage of 2.0 kV and a JEOL JEM-2100F transmission electron microscope (TEM). The selected area electron diffraction (SAED) pattern were taken with a JEOL JEM-2100F transmission electron microscope (TEM) and were used to evaluate the elemental composition of the produced materials. The X-ray photoelectron spectroscopy (XPS, K-alpha, Thermo Fisher) was used to analyse the elemental composition of the materials with a monochromatic Al-Kα radiation.

D. Electrodes preparation and characterization of supercapacitors

Three - and two electrode configurations were adopted to study the electrochemical properties of the VO_2 and C-FP electrodes.

The electrochemical characterizations were carried out using a Bio-Logic VMP-300 (Knoxville TN 37,930, USA) potentiostat monitored by the EC-Lab® V10.37 software. In the three-electrode configuration, Ag/AgCl (KCl saturated) served as the reference electrode, a glassy carbon plate as the counter electrode and 6 M KOH as the electrolyte. The VO_2 electrode was prepared as follows: 85 wt% of the active material was added to 10 wt% of carbon black as conducting additive and 5 wt% of polyvinylidene difluoride (PVDF) binder in an agate mortar. Few drops of 1-methyl-2-pyrrolidinone (NMP) were added to the mixture to form a slurry, which was pasted on nickel foam (NiF) acting as a current collector and dried at 60 °C in the electric oven for overnight.

Thereafter, the asymmetric supercapacitor consisting of VO_2 positive electrode and C-FP negative electrode was coupled in a coin cell with glass micro-fiber filter paper was used as a separator.

III. RESULTS AND DISCUSSION

A. Structural characterizations

Figure 1 display the X-ray diffraction patterns of VO_2 and C-FP materials. The diffraction peaks of the VO_2 materials are indexed as VO_2(B) monoclinic structure as shown in Fig. 1(a). It also shows that vanadium dioxide synthesized at 200 °C has a space group of *C 1 2/m 1*.[53] XRD pattern of C-FP powder material without pasting on the substrate (Ni foam) is shown in Fig. 1(b). The diffraction peaks of C-FP material are indexed to orthorhombic structures of Fe_3C and FeS with a space group of *P nma*.[54,55]

Figure 2 present the SEM micrographs of the as-prepared VO_2 and C-FP materials at low and high magnifications.

Figure 2(a) shows the SEM micrographs of the VO_2 which reveals the nanosheets-like structure on the microspheres surface. In Fig. (2b), the micrographs of VO_2 exhibits a vertically grown sheet-like structure. Figure 2(c–d) shows SEM micrographs of the C-FP which unveiled agglomerated nanograin morphology. The micrographs of the C-FP materials were showed lattice fringes attributed to the Fe cations on PANI and have been discussed in References 51 and 54.

The morphologies and the elemental composition of VO_2 materials were further studied with transmission electron microscope (TEM) and the selected area electron diffraction (SAED) analysis.

Figure 3(a) displays the TEM micrograph of VO_2 at high magnification which reveals clearly the nanosheets structure as shown in Fig. 2(b). The SAED pattern of the VO_2(B) nanosheets in Fig. 3(b) exhibits the presence of well-defined rings, indicates the poly-crystallinity of the VO_2 monoclinic.

To further evaluate the surface characterization of VO_2 material, the X-ray photoelectron spectroscopy (XPS) was used to determine the chemistry of the material. The core level spectrum of V*2p* reveals two chemical states of vanadium which are related to excitations of electrons from the V$2p_{3/2}$ and V$2p_{1/2}$ core levels, respectively, as shown in Fig. 4(a).

The predominant peak located at 516.5 eV in the V$2p_{3/2}$ binding energy suggests a vanadium oxidation state of 4^+ which confirms the formation of VO_2.[56] Futhermore, as presented in Fig. 4(b), the core level spectrum of O*1s* displayed the main peak located at 529.7 eV which is ascribed to the component associated to oxygen in VO_2.[57]

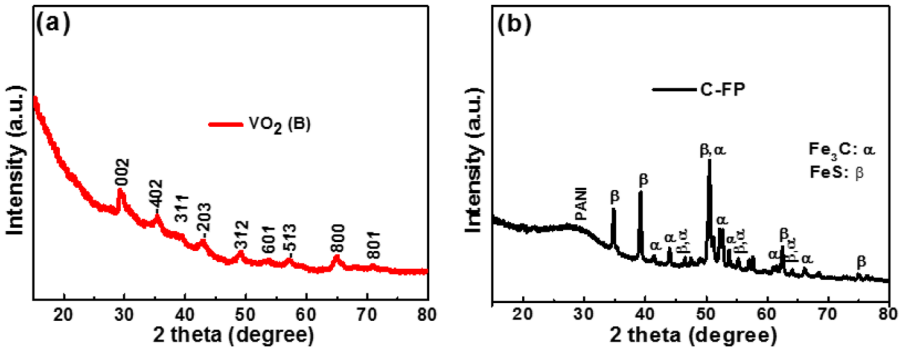

FIG. 1. The XRD patterns of (a) vanadium dioxide (VO_2) and (b) carbonized iron-polyaniline (C-FP).

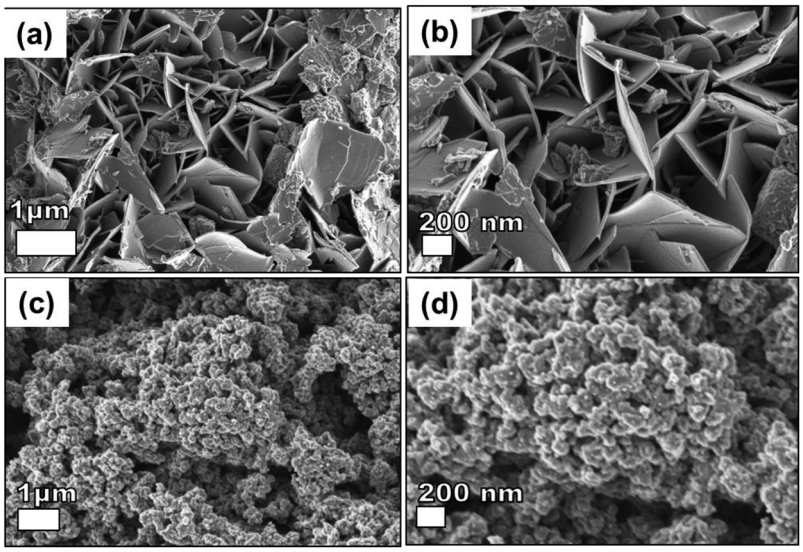

FIG. 2. The SEM images of the as-prepared (a-b) VO_2 and (c-d) C-FP at low and high magnifications.

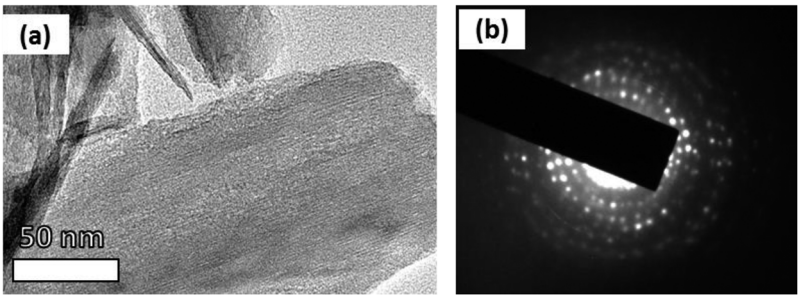

FIG. 3. (a) TEM at high magnification micrograph and (b) selected area electron diffraction (SAED) pattern of the VO_2 nanosheets.

B. Electrochemical performances of VO_2//C-FP

To construct the asymmetric hybrid supercapacitor of VO_2//C-FP, we, firstly, evaluated the electrochemical performance of the positive VO_2 and negative C-FP electrodes in a three-electrode system using 6 M KOH electrolyte with Ni foam and Ag/AgCl (KCl saturated) as a current collector and reference electrode, respectively.

Figure 5(a) shows the cyclic voltammogram (CV) profile of the VO_2 electrode at different sweep rates (from 5 to 100 mV s^{-1}) within a potential window range of 0.0 - 0.5 V. The appearance of a pair of redox peaks associated with an anodic peak at ~0.13 V and cathodic peak ~0.23 V at 5mV s^{-1} reveal a faradaic material. As observed in Fig. 5(a), these peaks are broader compared to those exhibited by battery-like material which is typically narrower and indicative of the occurrence of a redox reaction at a constant potential.[58]

The broadness of the peak in faradaic materials is expected as a result of the presence of non-standard sites and defects in the polycrystalline structure. This agrees with the low crystallinity of the VO_2 as recorded from XRD diffraction pattern.[58]

Figure 5(b) shows the charge-discharge (CD) of the vanadium dioxide curve at different specific currents. Each discharge curve displays a non-linear curve confirming the faradaic behavior of this electrode material.

Moreover, even at a low specific current of 1 A g^{-1}, the discharge profile does not show an extended plateau as is the case for batteries.[59] Figure 5(c) shows the CV curve of the C-FP electrode at different sweep rates from 5 to 100 mV s^{-1} in a negative potential window range of -1.2 - 0.0 V.

These CV curves show non-rectangular shapes with no apparent redox peaks. However, Fig. 5(d) which shows the charge-discharge curves at different specific currents in the voltage window of -1.2 to 0.0 V of the C-FP electrode, depicting a non-linear charge-discharge, suggesting a pseudocapacitive activity in this electrode material.

From the chronopotentiometry profile of the VO_2 and C-FP electrodes, the specific capacity, Q (measured in mA h g^{-1}) of the VO_2 and C-FP electrodes was determined using:

$$Q = \frac{I_d \times t_D}{3.6} \tag{1}$$

where I_d is defined as the specific current measured in A g^{-1} and t_D is the time in second (s) for a complete discharge cycle.

Figure 5(e) depicts the values of the specific capacity for the VO_2 and C-FP electrodes as a function of increasing specific current. The specific capacity values of 49.3 and 107 mA h g^{-1} were recorded for the VO_2 and C-FP material electrodes respectively, at a gravimetric current of 0.5 A g^{-1}. This can be related to the thin nanosheets structure of VO_2, which will ensure faster ion and electron transport. Also, the high capacitive characteristic observed in the C-FP can be attributed to the conductive framework, which allows an excellent electric contact and consequently enhances the capacitance performance. Additionally, it can be observed that these two materials (VO_2 and C-FP) are stable in each of its potential windows.

With the aim of optimizing the performance of ASC, the device was assembled using VO_2 as positive and C-FP as negative electrodes, respectively, in 6 M KOH.

The charge equilibrium ($Q_{VO_2(B)} = Q_{c-FP}$) was used to balance the masses of both electrodes in the asymmetric cell. This generates equation 2 and 3 which were used to balance the masses:

$$Q_{VO_2(B)} = Q_{c-FP} \tag{2}$$

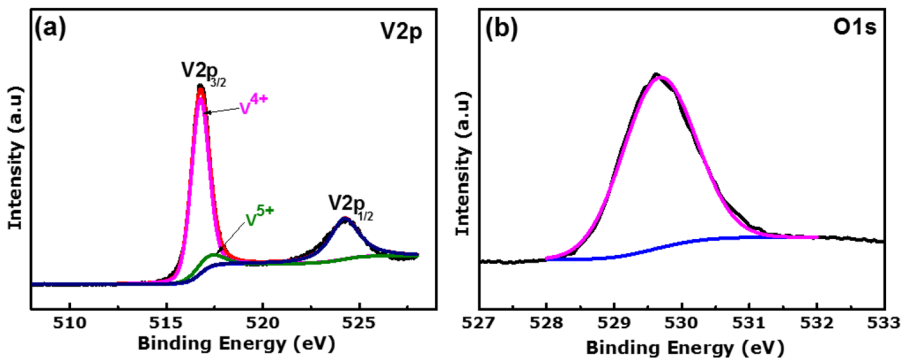

FIG. 4. (a) V2p binding energy region and (b) O1s binding energy regions of the VO_2 nanosheets.

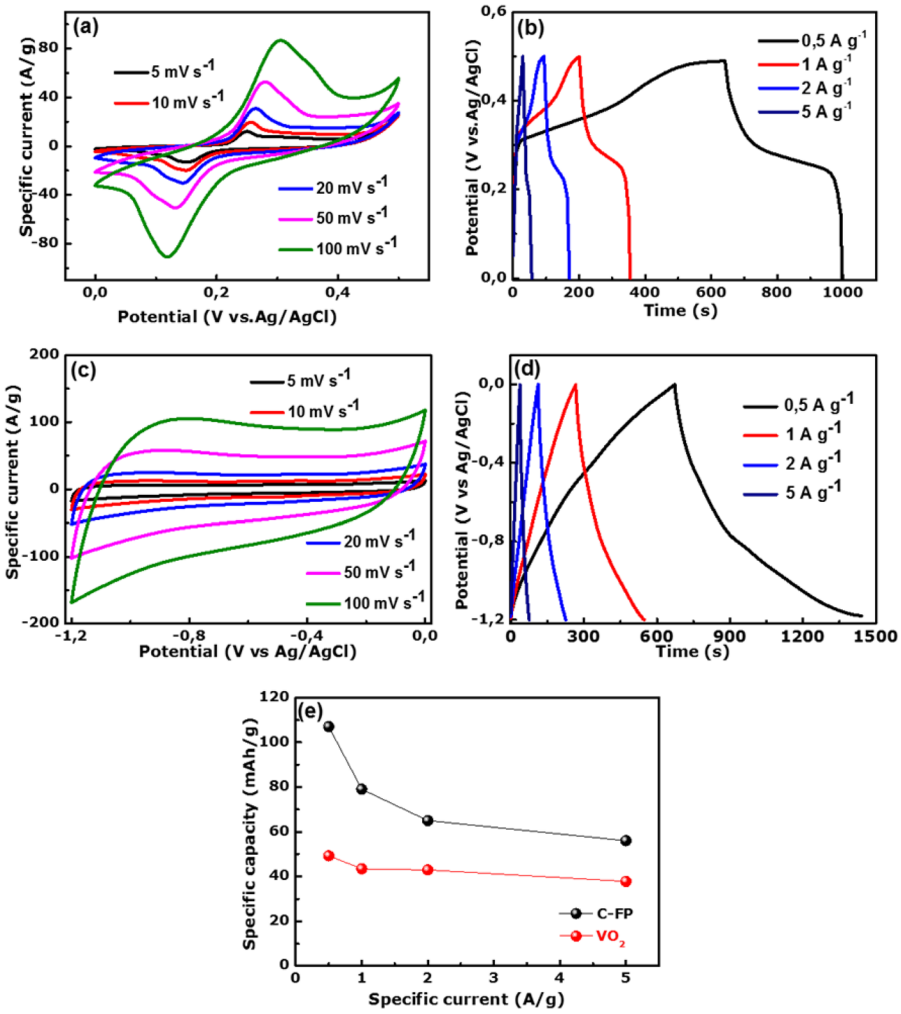

FIG. 5. (a) cyclic voltammogram (CV) curves at different sweep rates, (b) charge and discharge (CD) curves of the VO_2 at different specific current, (c) CV curves at different scan rates, (d) CD curves of the C-FP at different specific current and (e) specific capacities for the VO_2 and C-FP at different specific current.

$$\frac{m_{VO_2(B)}}{m_{c-FP}} = \frac{(I \cdot t_D)_{C-FP}}{(I \cdot t_D)_{VO_2(B)}} \tag{3}$$

where $m_{VO_2(B)}, m_{c-FP}, Q_{VO_2(B)}, Q_{c-FP}$ describes the mass loading and total charge of the VO_2 and C-FP electrodes, I is given as the applied current and t_D is the time of discharge to 0 V. The mass ratio of the VO_2 to C-FP was adopted as 2:1 and the mass loading per unit area of the VO_2 and C-FP electrodes was recorded as 2.24 and 1.12 mg cm^{-2}, respectively) According to the charge balance, the mass loading of active VO_2 and C-FP on the current collector were measured as 4 and 2 mg, respectively in line with equation 3 above.

Figure 6(a) shows the CV curves of VO_2 and C-FP measured in the stable working potential window at a sweep rate of 50 mV s^{-1}, a working potential window of 1.7 V could be predicted for the asymmetric device.

Figure 6(b) shows the CV graphs of the VO_2//C-FP asymmetric device at different sweep rates (5 to 200 mV s^{-1}). However, the maximum working potential limit of the VO_2//C-FP device was recorded to be 1.6 V.

There is no apparent current leap within the operating cell potential window of 1.6 V, suggesting the stability of the device within this potential window. The CD curves of VO_2//C-F at different specific currents (1 to 10 Ag^{-1}) are shown in Fig. 6(c). The CD curves exhibit faradaic behavior owing to the high redox activity observed from the CV curves of the asymmetric device. The specific capacity of the VO_2//C-FP device was calculated using equation (1) and is shown in Fig. 6(d) as a function of specific current.

The specific capacity of the VO_2//C-FP device reaches a value of 47 mA h g^{-1} at a gravimetric current of 1 A g^{-1}. This value is well positioned between those obtained for VO_2 and C-FP electrodes from the three electrode measurements, at the same specific current. In other words, the specific capacity value of the hybrid device is much higher than that of VO_2 (43.4 mA h g^{-1}) and lower than that of C-FP (79 mA h g^{-1}) calculated in the three-electrode configuration at a gravimetric current of 1 A g^{-1}. This shows a good synergistic improvement by combining these two materials to form a hybrid device.

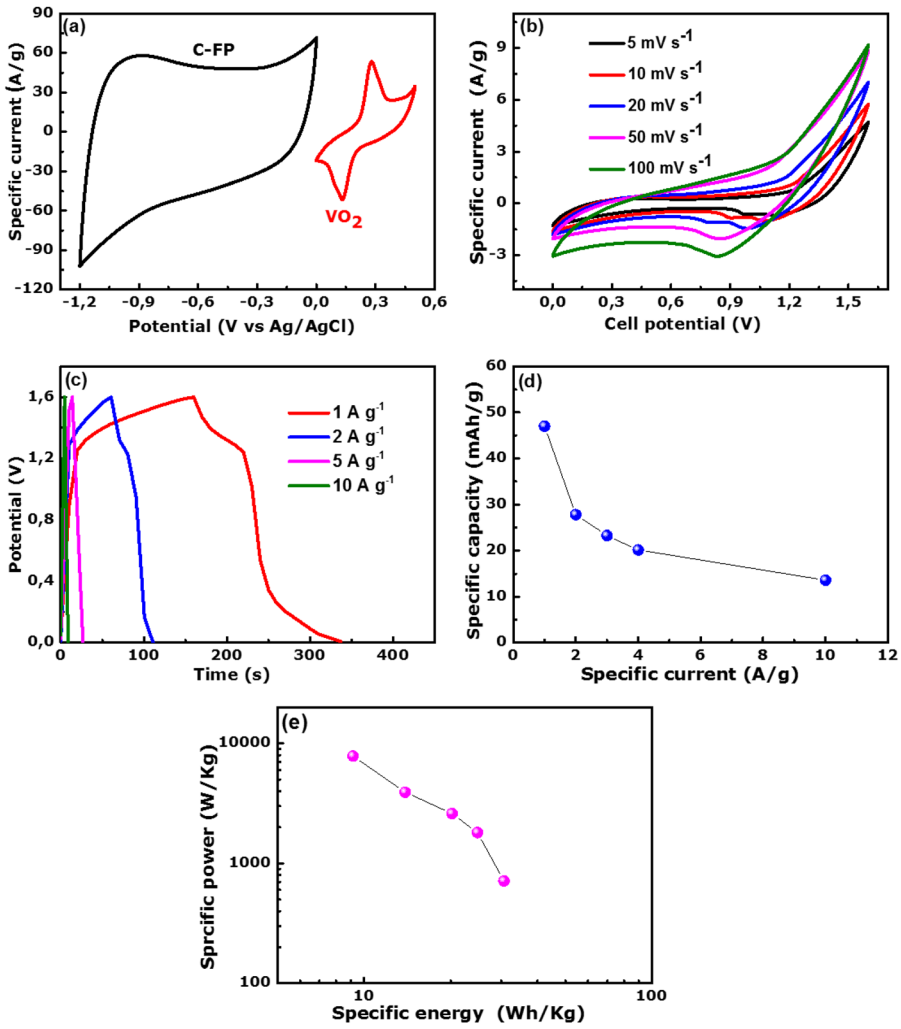

FIG. 6. (a) cyclic voltammograms (CVs) of VO_2 and C-FP electrodes at 50 mV s^{-1} for three-electrode setup, for the asymmetric device of the VO_2//C-FP (b) CV, (c) CD and (d) specific capacity at different specific current and (e) Ragone plot.

Figure 6(e) displays the Ragone plot presenting the specific power versus the specific energy of the asymmetric device obtained at different specific currents. The specific energy and the specific power of the device were obtained using equations (4) and (5) respectively.[60]

$$E_d(\mathrm{W\,h\,kg^{-1}}) = \frac{I_d}{3.6}\int V(t)dt \tag{4}$$

$$P_d(\mathrm{W\,kg^{-1}}) = 3600\frac{E_D}{t} \tag{5}$$

where E_d (W h kg^{-1}) and P_d (W kg^{-1}) are the total specific energy and specific power respectively. I_d is the specific current in A g^{-1}, t is the discharge time (s) and V is the working potential window (V) of the $V0_2$//C-FP device.

The maximum specific energy value of 30 Wh kg^{-1} was recorded for the VO_2//C-FP device with an associated specific power value of 713 W kg^{-1} at a 1 A g^{-1} specific current. This is maintained at 9.1 W h kg^{-1} for a specific power of 7.9 kW kg^{-1} at 10 A g^{-1}. The high specific energy and specific power of the ASC are attributed to a high specific capacity and device wide operating voltage. This is also related to the good stability, fast kinetics of charge/discharge process[61] and the high ionic conductivity of the electrolyte ions, i.e., 73.5 and 198 Scm^2 mol^{-1} for K^+ and OH^-, respectively.[26]

In order to study the stability of the device, it was subjected to 10000 cycles at the high gravimetric current of 10 A g^{-1} and the results are shown in Fig. 7(a).

An energy efficiency of the device was calculated using equation (6)

$$\eta_E = \frac{E_d}{E_c} \times 100 \tag{6}$$

where η_E, E_d and E_c are energy efficiency, discharge energy and charge energy from the charge-discharge curve of the VO_2//C-FP device respectively.

The energy efficiency of 89% is obtained with good capacity retention of 78.5% at the 10 000th constant charge-discharge cycle, signifying good electrochemical stability of the device. The further

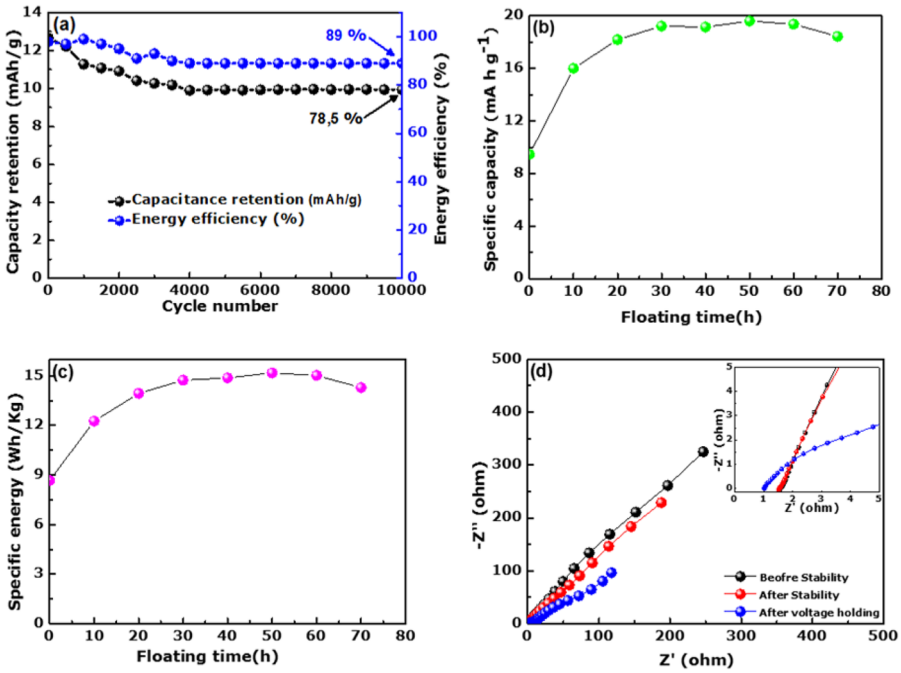

FIG. 7. (a) Stability test showing energy efficiency and capacity retention for up to 10000th cycles at a constant gravimetric current of 10 A g^{-1}, (b) specific capacity as function of floating time at 10 A g^{-1}, (c) specific energy as function of holding time at 10 A g^{-1}, (d) EIS before and after 10000th cycles and 70h voltage holding of the VO_2//C-FP asymmetric cell.

additional stability test was performed after cycling measurement on the cell using the voltage holding test (also called floating test).[62] It has the ability to determine a direct insight into the possible effect and degradation phenomena which might occur during the electrochemical process.[63] The voltage holding test was designed to analyse the device specific capacity at each 10 h period of the potential holding step for up to 70 h. This is following by three GCD to exhibit any change in the cell device with floating over a time of 70 h. The specific capacity as a function of floating time is presented in Fig. 7(b) for 70 h at 10 A g^{-1}.

It exhibits an increase in the specific capacity value for up to 30 h period of voltage holding time before becoming constant. The increase in the specific capacity could be linked to the evolution of accessible redox sites during the ageing experiment.

This improvement is even more striking when the specific energy was calculated after each voltage holding as shown in Fig. 7(c). Within the first 10 h of voltage holding, the specific energy increases by 32% to finally stabilize after 30 h of floating test, at 15 W h kg^{-1}, corresponding to an impressive increase of 65% from the original 9.1 W h kg^{-1} at 10 A g^{-1}. It shows that the cell voltage (1.6 V) is stable using 6 M KOH. As compared to other hybrid devices our group has reported this increase is better than that of $Co_3(PO_4)_2{\cdot}4H_2O$/GF//C-FP (2.2% from the original value of 9.1 Wh Kg^{-1})[64] as earlier reported for hybrid asymmetric capacitors. Thus, the floating test should be considered as a viable option for optimizing the properties of this cell.

The electrochemical impedance spectroscopic (EIS) measurement of the device was performed in an open voltage from 0.01 Hz to 100 kHz frequencies. The Nyquist plot of the asymmetric device (VO_2//C-FP), before stability, after the 10.000 constant galvanostatic cycles and after voltage holding are shown in Fig. 7(d). The equivalent series resistance (ESR) value of the asymmetric device (VO_2//C-FP) was 1.55 Ω before and after 10000th cycles. However, after voltage holding, the ESR decreased to 1 Ω followed by a shorter diffusion length of the electrolyte ions. This low value of ESR confirm the good contact between the electrolyte and the surface of the electrode materials. Thus, any degradation of the cell has been not observed after the voltage holding. More explicitly, no change in the equivalent series resistance was noticed after stability. Two main changes in the impedance could explain the electrochemical improvement of the cell after voltage holding. However, the diffusion was reduced after the stability test. Upon voltage holding, the diffusion length is markedly reduced followed by reduction of the solution resistance. These reductions can significantly enhance the performance of the cell by a fast collection of charges.

Table I compares the asymmetric VO_2//C-FP device with some others devices reported in the literature. The cell shows higher

TABLE I. Comparison of electrochemical properties of VO_2//C-FP with previous supercapacitors comprised of VO_2.

Materials	Specific current (A/g)	Specific energy (Wh/Kg)	Specific power (W/Kg)	References
GF(0.1)/VO_2//GF	0.25	22.8	425	4
VO_2//VO_2	0.25	21.3	207.2	48
Graphene/VO_2// graphene/VO_2	1	21.3	-	52
GF+VO_2//HMB	2	14.5	720	65
VO_2//C-FP	**1** **2**	**30** **25**	**713** **1806**	**This work**

values when compared with other devices.[4,48,52,65] This demonstrates the excellent choice of tandem materials for this asymmetric device.

IV. CONCLUSIONS

We have successfully synthesized VO_2(B) nanosheets by a solvothermal method and C-FP material by pyrolysis of an iron-PANI mixture under nitrogen atmosphere. An ASC cell was fabricated from VO_2 adopted as positive and C-FP as the negative electrodes operated with an aqueous 6 M KOH electrolyte. The asymmetrical device exhibited a specific capacity of 47 mA h g^{-1} with a high specific energy of 30 W h kg^{-1} and the corresponding specific power of 713 W kg^{-1} at 1 A g^{-1} with 1.6 cell potential. These values are far better as compared to those studies previously published for related devices as indicated in Table I above. The excellent stability performance of the VO_2//C-FP device was demonstrated up to 10000 cycles at a specific current of 10 A g^{-1}. In addition, the voltage holding data obtained after testing for a period of 70 h shows a significant improvement in device specific capacity and energy after a period of 10 h at 10 A g^{-1}. This result confirms that the performance of the VO_2//C-FP device increase after the voltage holding test. This asymmetric supercapacitor from VO_2//C-FP exhibits impressive electrochemical performance and hence making the device excellent for energy storage applications.

ACKNOWLEDGMENTS

This research was supported by the South African Research Chairs Initiative (SARChI) of the Department of Science and Technology and the National Research Foundation (NRF) of South Africa (Grant No. 61056). Any idea, finding, conclusion or recommendation expressed in this material is that of the author(s). The NRF does not accept any liability in this regard. N. M. Ndiaye thanks Organization for Women in Science for the Developing World (OWSD) and Swedish International Development Cooperation Agency (Sida), NRF through SARChI in Carbon Technology and Materials and the University of Pretoria for financial support.

REFERENCES

[1] W. Y. Tsai, P. C. Gao, B. Daffos, P. L. Taberna, C. R. Perez, Y. Gogotsi, F. Favier, and P. Simon, Electrochemistry Communications **34**, 109 (2013).
[2] H. Li, B. Wang, X. He, J. Xiao, H. Zhang, Q. Liu, J. Liu, J. Wang, L. Liu, and P. Wang, J. Mater. Chem. A **3**, 9754 (2015).
[3] P. Simon and Y. Gogotsi, Nat. Mater. **7**, 845 (2008).
[4] L. Deng, G. Zhang, L. Kang, Z. Lei, C. Liu, and Z.-H. H. Liu, Electrochimica Acta **112**, 448 (2013).
[5] P. S. J. R. Miller, J. Miller, P. Simon, and P. S. J. R. Miller, Science **321**, 651 (2008).
[6] B. E. Conway, Kluwer Academic **10**, 221 (1999).
[7] Z. Yu, L. Tetard, L. Zhai, and J. Thomas, Energy Environ. Sci. **8**, 702 (2015).
[8] P. Simon, Y. Gogotsi, and B. Dunn, Science **343**, 1210 (2014).
[9] B. E. Conway, Journal of the Electrochemical Society **138**, 1539 (1991).
[10] J. T. Mefford, W. G. Hardin, S. Dai, K. P. Johnston, and K. J. Stevenson, Nature Materials **13**, 726 (2014).
[11] Y. Xiao, W.-Y. Wang, S.-W. Chou, T.-W. Lin, and J.-Y. Lin, Journal of Power Sources **266**, 448 (2014).
[12] M.-N. Lu, C.-S. Dai, S.-Y. Tai, T.-W. Lin, and J.-Y. Lin, Journal of Power Sources **270**, 499 (2014).
[13] T.-W. Lin, M.-C. Hsiao, S.-W. Chou, H.-H. Shen, and J.-Y. Lin, Journal of the Electrochemical Society **162**, A1493 (2015).
[14] B. Rong-Rong, W. Xing-Long, C. Fei-Fei, J. Ling-Yan, G. Yu-Guo, and W. Li-Jun, The Journal of Physical Chemistry C **114**, 2448 (2010).
[15] H. Jiang, C. Li, T. Sun, and J. Ma, Nanoscale **4**, 807 (2012).
[16] J. Zhu, L. Huang, Y. Xiao, L. Shen, Q. Chen, and W. Shi, Nanoscale **6**, 6772 (2014).
[17] J.-W. Lang, L.-B. Kong, W.-J. Wu, Y.-C. Luo, and L. Kang, Chemical Communications **104**, 4213 (2008).
[18] L.-M. M. Chen, Q.-Y. Y. Lai, Y.-J. J. Hao, Y. Zhao, X.-Y. Y. Ji, Y. Z. Lian-Mei Chen, Q.-Y. Lai, H. Yan-Jing, and X.-Y. Ji, Journal of Alloys and Compounds **467**, 465 (2009).
[19] W. Xiao, *Asymmetric Capacitor Based on Vanadium Dioxide/Graphene/Nickle and Carbon Nanotube Electrode* (University of Akron, 2014).
[20] A. Rudge, J. Davey, I. Raistrick, S. Gottesfeld, and J. P. Ferraris, Journal of Power Sources **47**, 89 (1994).
[21] H. Li, Y. Gao, C. Wang, and G. Yang, Advanced Energy Materials **5**, 1401767 (2015).
[22] J. Huang, P. Xu, D. Cao, X. Zhou, S. Yang, Y. Li, and G. Wang, Journal of Power Sources **246**, 371 (2014).
[23] R. R. Salunkhe, J. Lin, V. Malgras, S. X. Dou, J. H. Kim, and Y. Yamauchi, Nano Energy **11**, 211 (2015).
[24] J. Yan, Z. Fan, W. Sun, G. Ning, T. Wei, Q. Zhang, R. Zhang, L. Zhi, and F. Wei, Advanced Functional Materials **22**, 2632 (2012).
[25] B. G. Choi, S.-J. Chang, H.-W. Kang, C. P. Park, H. J. Kim, W. H. Hong, S. Lee, and Y. S. Huh, Nanoscale **4**, 4983 (2012).
[26] Y.-G. Wang, L. Cheng, and Y.-Y. Xia, Journal of Power Sources **153**, 191 (2006).
[27] D. P. Dubal, O. Ayyad, V. Ruiz, and P. Gómez-Romero, *Hybrid Energy Storage: The Merging of Battery and Supercapacitor Chemistries* (Royal Society of Chemistry, 2015), pp. 1777–1790.
[28] D. Salinas-Torres, J. M. Sieben, D. Lozano-Castelló, D. Cazorla-Amorós, and E. Morallón, Electrochimica Acta **89**, 326 (2013).
[29] Q. Wang, J. Yan, Y. Wang, G. Ning, Z. Fan, T. Wei, J. Cheng, M. Zhang, and X. Jing, Carbon **52**, 209 (2013).
[30] Y. Fang, B. Luo, Y. Jia, X. Li, B. Wang, Q. Song, F. Kang, and L. Zhi, Advanced Materials **24**, 6348 (2012).
[31] L. L. Zhang and X. S. Zhao, Chemical Society Reviews **38**, 2520 (2009).
[32] W. F. Mak, G. Wee, V. Aravindan, N. Gupta, S. G. Mhaisalkar, and S. Madhavi, Journal of the Electrochemical Society **159**, A1481 (2012).
[33] E. Umeshbabu and G. Ranga Rao, Journal of Colloid and Interface Science **472**, 210 (2016).
[34] H. Zhao, L. Pan, S. Xing, J. Luo, and J. Xu, Journal of Power Sources **222**, 21 (2013).
[35] M. H. Bai, L. J. Bian, Y. Song, and X. X. Liu, ACS Applied Materials and Interfaces **6**, 12656 (2014).
[36] X. Pan, G. Ren, M. N. F. Hoque, S. Bayne, K. Zhu, and Z. Fan, Advanced Materials Interfaces **1**, 1400398 (2014).
[37] H. Li, K. Jiao, L. Wang, C. Wei, and B. Xie, Journal of Materials Chemistry A: Materials for Energy and Sustainability **2**, 18806 (2014).
[38] G. P. Nagabhushana and G. T. Chandrappa, Journal of Materials Chemistry A **1**, 11539 (2013).
[39] I. Derkaoui, M. Khenfouch, I. Elmokri, S. J. Moloi, B. M. Mothudi, M. S. Dhlamini, M. Maaza, I. Zorkani, and A. Jorio, Graphene **5**, 14 (2016).
[40] S. Kachi, T. Takada, and K. Kosuge, Journal of the Physical Society of Japan **18**, 1839 (1963).
[41] H. Hosseini and S. Shahrokhian, Applied Materials Today **10**, 72 (2018).
[42] S. Rao Popuri, A. Artemenko, C. Labrugere, M. Miclau, A. Villesuzanne, and M. Pollet, Journal of Solid State Chemistry **213**, 79 (2014).
[43] Y. Wang and Z. Zhang, Physica E: Low-Dimensional Systems and Nanostructures **41**, 548 (2009).
[44] Y. Oka, S. Sato, T. Yao, and N. Yamamoto, Journal of Solid State Chemistry **141**, 594 (1998).
[45] X. Pan, Y. Zhao, G. Ren, and Z. Fan, Chemical Communications **49**, 3943 (2013).
[46] S. Surnev, M. G. Ramsey, and F. P. Netzer, Progress in Surface Science **73**, 117 (2003).

[47]X. Xiao, S. Li, H. Wei, D. Sun, Y. Wu, G. Jin, F. Wang, and Y. Zou, Journal of Materials Science: Materials in Electronics **26**, 4226 (2015).
[48]X.-J. J. Ma, W.-B. Bin Zhang, L.-B. Bin Kong, Y.-C. C. Luo, and L. Kang, RSC Advances **5**, 97239 (2015).
[49]K. Tang, Y. Li, Y. Li, H. Cao, Z. Zhang, Y. Zhang, and J. Yang, Electrochimica Acta **209**, 709 (2016).
[50]L. Danxia, H. Wanxia, S. Linwei, and S. Qiwu, Advanced Materials Research **1120**, 158 (2015).
[51]Y. Oka, T. Yao, and N. Yamamoto, Journal of Solid State Chemistry **86**, 116 (1990).
[52]H. Wang, H. Yi, X. Chen, X. Wang, D. W. Liu, J. Liu, G. Z. Cao, P. M. Ajayan, and F. Wei, Journal of Materials Chemistry A **2**, 1165 (2014).
[53]N. M. M. Ndiaye, T. M. M. Masikhwa, B. D. D. Ngom, M. J. J. Madito, K. O. O. Oyedotun, J. K. K. Dangbegnon, and N. Manyala, Materials Chemistry and Physics **214**, 192 (2018).
[54]M. N. Rantho, M. J. Madito, and N. Manyala, Electrochimica Acta **262**, 82 (2018).
[55]T. M. Masikhwa, D. Y. Momodu, K. O. Oyedotun, A. A. Mirghni, N. M. Ndiaye, and N. Manyala, Journal of Alloys and Compounds **769**, 376 (2018).
[56]C.-T. Wang and H.-H. Huang, Journal of Non-Crystalline Solids **354**, 3336 (2008).
[57]E. Z. Kurmaev, V. M. Cherkashenko, Y. M. Yarmoshenko, S. Bartkowski, A. V Postnikov, M. Neumann, L.-C. Duda, J. H. Guo, J. Nordgren, V. A. Perelyaev, and W. Reichelt, Journal of Physics: Condensed Matter **10**, 4081 (1998).
[58]A. Eftekhari and M. Mohamedi, Materials Today Energy **6**, 211 (2017).
[59]A. Eftekhari, Sustainable Energy & Fuels **1**, 2053 (2017).
[60]X. X. Wang, Y. Zhang, C. Zhi, X. X. Wang, D. Tang, Y. Xu, Q. Weng, X. Jiang, M. Mitome, D. Golberg, and Y. Bando, Nature Communications **4**, 2905 (2013).
[61]A. Leela Mohana Reddy, F. Estaline Amitha, I. Jafri, and S. Ramaprabhu, Nanoscale Research Letters **3**, 145 (2008).
[62]D. Weingarth, H. Noh, A. Foelske-Schmitz, A. Wokaun, and R. Kötz, Electrochimica Acta **103**, 119 (2013).
[63]A. Bello, F. Barzegar, M. J. Madito, D. Y. Momodu, A. A. Khaleed, T. M. Masikhwa, J. K. Dangbegnon, and N. Manyala, Electrochimica Acta **213**, 107 (2016).
[64]A. A. Mirghni, D. Momodu, K. O. Oyedotun, J. K. Dangbegnon, and N. Manyala, Electrochimica Acta **283**, 374 (2018).
[65]X. Xia, D. Chao, C. F. Ng, J. Lin, Z. Fan, H. Zhang, Z. X. Shen, and H. J. Fan, Mater. Horiz. **2**, 237 (2015).